Inorganic Chemistry
Article
pubs.acs.org/IC

Highly Efficient Cuprous Complexes with Thermally Activated Delayed Fluorescence for Solution-Processed Organic Light-Emitting Devices

Dong Liang,[†,‡] Xu-Lin Chen,[†] Jian-Zhen Liao,[†,‡] Jin-Yu Hu,[†,‡] Ji-Hui Jia,[†,§] and Can-Zhong Lu*,[†]

[†]Key Laboratory of Design and Assembly of Functional Nanostructures, Fujian Institute of Research on the Structure of Matter, Chinese Academy of Science, Fuzhou, Fujian 350002, People's Republic of China

[‡]University of Chinese Academy of Sciences, Beijing, 100049, China

[§]College of Materials Science and Engineering, Fujian Normal University, Fuzhou, Fujian 350007, People's Republic of China

S *Supporting Information*

ABSTRACT: Two mononuclear cuprous complexes $[Cu(PNNA)(POP)]BF_4$ (**1**) and $[Cu(PNNA)(Xantphos)]BF_4$ (**2**) (PNNA = 9,9-dimethyl-10-(6-(3-phenyl-1*H*-pyrazol-1-yl)pyridin-3-yl)-9,10-dihydroacridine, POP = bis[2-(dipenylphosphino)phenyl]ether, Xantphos =4,5-bis-(diphenylphosphino)-9,9-dimethylxanthene), with intense bluish-green luminescence based on a new diimine ligand were designed and synthesized. Their structural, electrochemical, and photophysical properties were characterized by single-crystal X-ray analysis, cyclic voltammetry, temperature dependence of spectroscopy, time-dependent emission spectroscopy, etc. The complexes exhibit high photoluminescence quantum yields in doped films (up to 74.6%) at room temperature. Thermally activated delayed fluorescence based on intraligand charge transfer was observed by grafting a strong electron-donor moiety, 9,9-dimethylacridan, on the diimine ligand, which is supported by the density functional theory calculations on two complexes. Highly efficient solution-processed OLEDs based on these two complexes were fabricated, among which the electroluminescent device using **2** as dopant shows a peak external quantum efficiency of 7.42%, a peak current efficiency of 20.24 cd/A, and a maximum brightness of 5579 cd/m^2.

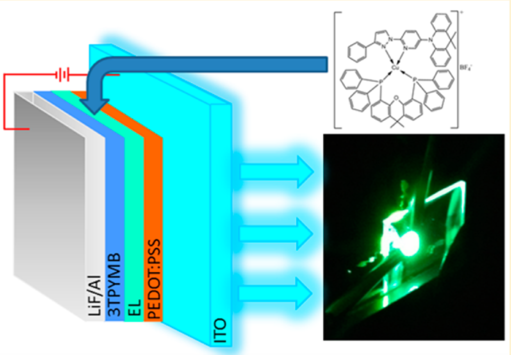

INTRODUCTION

Over the past decades, organic light-emitting diodes (OLEDs) have drawn considerable attention because of their unique advantages in lighting and display applications. On one hand, researchers have struggled in finding luminescent dopants which can fully utilize all excitons from two excited states (singlet and triplet states) for luminescence in OLEDs. Thus far, phosphorescent organometallic complexes based on platinum group metals are the most common dopants to achieve highly efficient OLEDs.[1−3] Theoretically, 100% internal quantum efficiency can be realized in these phosphorescent complexes because excitons of the lowest triplet state (T_1) are relatively allowed to transit to the ground state (S_0) due to the high spin−orbit coupling (SOC) which is induced by the heavy metal atoms. However, disadvantages of these complexes, such as high cost, limited availability, and lack of highly efficient blue-emitting phosphorescent emitters, limit the commercialization of phosphorescent OLEDs. Recently, a lot of research has been directed toward the discovery of low-cost and more abundant alternatives, among which cuprous complexes have been proved to be promising candidates.[4−13] Because of the distinct spatial separations of the highest occupied molecular orbital (HOMO) and lowest unoccupied molecular orbital (LUMO), many cuprous complexes possess small energy gaps ΔE_{ST} between the lowest excited singlet states (S_1) and the lowest triplet states (T_1). The small energy gaps ΔE_{ST} ensure efficient upconverting triplet excitons into singlet excited states, resulting in efficient TADF emission.[14−19] At the same time, cuprous complexes frequently show high photoluminescence quantum yields (PLQYs) by introducing significant steric hindrance on the ligands.[20−23] Theoretically, due to the small ΔE_{ST} and high PLQYs of the cuprous complexes, we can obtain luminescent materials with high internal electroluminescence efficiencies compared with those of the noble-metal phosphorescent materials.

On the other hand, optimization of device structures is another crucial aspect for developing high-performance and low-cost OLEDs. Compared with vacuum vapor deposition, solution processing is a more satisfying way for fabricating commercialized devices because of its potential in low-cost as well as large area manufacturing processes, for instance, spin coating and inkjet printing. Moreover, multidopant devices, e.g., white-light OLEDs, can be much more easily fabricated via

Received: March 28, 2016

DOI: 10.1021/acs.inorgchem.6b00763

Scheme 1. Synthetic Route of Diimine Ligand PNNA

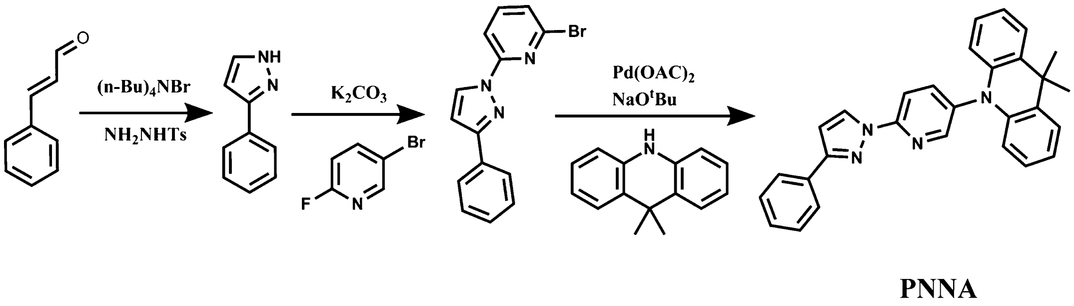

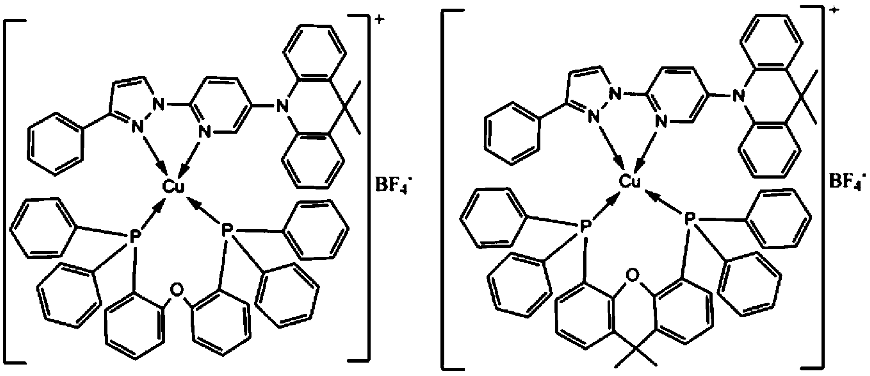

Figure 1. Molecular structure of cuprous complexes **1** (left) and **2** (right).

solution processing.[24−28] However, because the solubility of each functional layer must be different from each other, a multilayer device is difficult to be formed by solution processing. As a consequence, the injecting and transporting balance of holes and electrons in solution-processed OLEDs is usually difficult to realize by stacking different functional layers. This obstacle can be overcome by using multifunctional materials in some layers. Multifunctional hosts and dopants are frequently used in emitting layers to balance the transporting of carriers. For instance, the carbazole modules with excellent characteristics of hole transporting and high triplet levels have been widely integrated into Ir(III) complexes and host materials for highly efficient OLEDs.[29−33] However, this strategy has been rarely adopted in OLEDs based on luminescent cuprous complexes so far.

In this paper, we present two strongly bluish-green-emitting Cu(I) complexes, [Cu(PNNA)(POP)]BF_4 (**1**) and [Cu(PNNA)(Xantphos)]BF_4 (**2**), which show efficient TADF emission at room temperature. In order to improve PLQYs by restraining the fattening distortion in the excited states and at the same time improve the hole-transporting abilities, we integrated a diimine ligand with 9,9-dimethylacridan which possesses large steric hindrance and excellent hole-transporting property. 9,9-Dimethylacridan has been widely used as a donor moiety in pure organic TADF materials due to its strong electron donor ability and high triplet level. The luminescence of most cuprous complexes stems from metal to ligand charge transfer (MLCT) transitions. Compared with pure organic TADF materials, the metal centers of these complexes act as donor parts of pure organic emitters, while ligands act as the acceptors. However, when the strong electron donor, i.e., 9,9-dimethylacridan, is introduced in the diimine ligand, the titled cuprous complexes unusually exhibit ILCT-based emission. High performances have been demonstrated for cost-effective solution-processed OLEDs based on these cuprous complexes.

■ RESULTS AND DISCUSSION

Synthesis and Characterization. Scheme 1 shows the synthetic route of the diimine ligand PNNA. This ligand can be easily prepared by three steps with a moderate overall yield.

The cuprous complexes **1** and **2** were prepared by reactions of [$Cu(CH_3CN)_4$]BF_4, PNNA, and the corresponding phosphine ligands. Molecular structures of the two complexes are shown in Figure 1. They were characterized by ^1H NMR, ^{31}P NMR, and elemental analysis. In order to evaluate the stability of these complexes in solution, mass spectra (MS) (Figure S1, Supporting Information) and UV−vis absorption spectra (Figure S2, Supporting Information) were carried out for solution samples which had been exposed to air for 10 days. The results demonstrate that these complexes are stable even in solution under air. Moreover, single crystals of these complexes can still be obtained from the exposed solution samples. Thermal gravimetric analysis (TGA) was carried out to evaluate the thermal stability of powder samples. The decomposition temperatures T_d, corresponding to a weight loss of 5%, are 341 °C for **1** and 347 °C for **2** (Figure S3, Supporting Information). Such high decomposition temperatures are believed to be beneficial to device fabricating.

Single crystals suitable for X-ray diffraction analysis were obtained by the diffusion of diethyl ether into CH_2Cl_2 solutions of the complexes. The crystal structures of two complexes have been determined by single-crystal X-ray diffraction analysis, and their ORTEP diagrams are shown in Figure 2. Selected bond lengths and angles are listed in Table S2 in the Supporting Information. These cuprous complexes display irregular tetrahedral coordination with bond angles of ∠N−Cu−N = 79.12° and ∠P−Cu−P = 116.34° for **1** and ∠N−Cu−N = 78.31° and ∠N−Cu−N = 121.64° for **2**.

Photophysical Properties. Figure 3 shows UV−vis absorption and emission spectra of the complexes in degassed

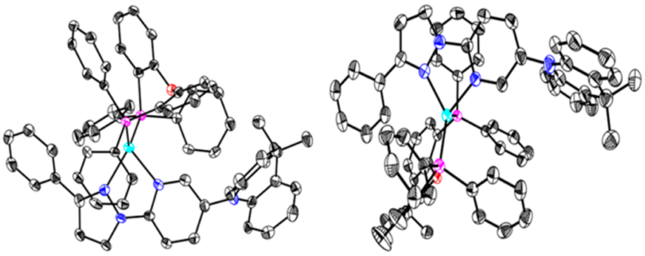

Figure 2. Crystal structures of complexes **1** (left) and **2** (right).

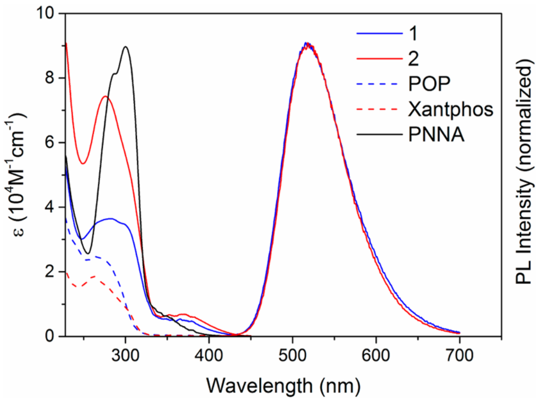

Figure 3. Absorption spectra (left) of the cuprous complexes and free ligands in degassed CH_2Cl_2 ($c \approx 2 \times 10^{-5}$) and emission spectra (right) of the cuprous complexes in degassed CH_2Cl_2 measured at room temperature (λ_{exc} = 370 nm).

CH_2Cl_2 together with absorption spectra of the free ligands in degassed CH_2Cl_2. These cuprous complexes exhibit intense absorption bands between 250 and 325 nm, which are attributed to spin-allowed π–π* transition of both the PNNA and the phosphine ligands.[34]

The weak absorption bands (325–400 nm) of two cuprous complexes, which are also observed for the free diimine ligand, can be mainly attributed to intraligand charge transfer (ILCT) transition. This assignment is supported by the results of density functional theory (DFT) calculations on two complexes, which reveal that the electron density of the HOMO is distributed over the acridine part of the diimine ligand and the LUMO is mainly localized on the other part of the diimine ligand. According to the frontier orbital analyses (Figure 4), these cuprous complexes exhibit substantial ILCT character which is different from the common MLCT nature for most cuprous complexes hitherto studied. As a comparison, the ligand PNNA shows a similar ILCT character, while it possesses a much wider optical band gap (E_g) than those of complexes **1** and **2**.

As depicted in Figure 3, the emission spectra of these cuprous complexes in degassed CH_2Cl_2 are almost the same. Both of them emit bright yellow-green light under excitation with UV light. The PLQYs of complexes **1** and **2** in degassed CH_2Cl_2 are 16% and 19%, respectively. The Stokes shifts, which are defined as the distance between individual excitation and emission spectra maxima, are 148 and 145 nm for **1** and **2**, respectively. The intense luminescence in solution and small Stokes shifts relative to many four-coordination cuprous complexes can be attributed to significant steric hindrance of the ligands in these complexes which obstructs efficiently the structural flattening distortion at the excited state. In a more rigid matrix, the geometry distortion combined with the nonradiative quenching process in the excited state can be further suppressed, which lead to more efficient emission. For example, complexes **1** and **2** show strong luminescence with PLQYs up to 69.9% and 74.6% in doped mCP film, respectively.

Figure 5 shows the emission spectra of powder samples at 293 and 77K. The photophysical data of the cuprous complexes are summarized in Table 1. At 293 K, complexes **1** and **2** both emit strong bluish-green luminescence, which show individually emissions at 493 and 475 nm with short lifetimes of 145 and 51 μs, respectively. The red-shifting emissions accompanied by lengthening lifetimes are observed when temperature decreases. At 77 K, two complexes exhibit red-shifted emissions at maximum emission wavelengths of 501 (for **1**) and 516 nm (for **2**) with longer lifetimes of 593 (for **1**) and 496 μs (for **2**). These observations indicate that luminescence of these complexes at 77 and 293 K may result from individually interconvertible excited states in thermal equilibrium, respectively. To further investigate the decay behavior and nature of the excited states of these cuprous complexes, lifetimes at different temperatures between 77 and 373 K were measured. In a situation of a fast thermal equilibrium between the S_1 and the T_1 sates, the observed decay time (τ_{obs}) of the complexes which depends on temperature can be described by the following equation[19]

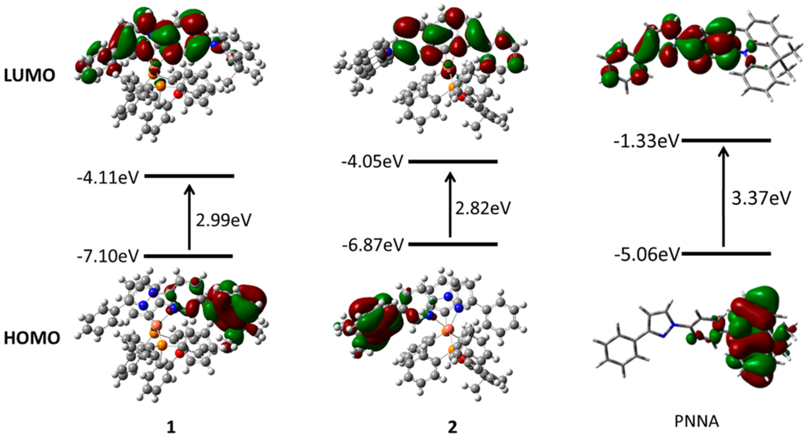

Figure 4. Frontier molecular orbitals for complexes **1**, **2**, and **PNNA** with their relative energies from DFT calculations.

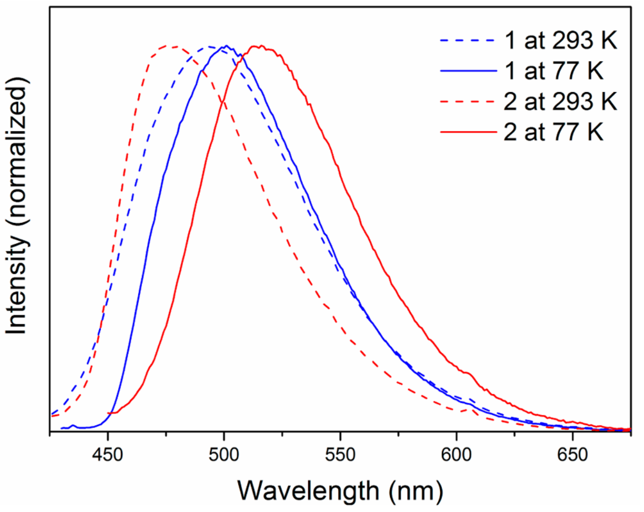

Figure 5. Emission spectra of the cuprous complexes as powders at different temperatures (λ_{exc}= 370 nm).

$$\tau_{obs} = \frac{1 + \frac{1}{3}\exp\left(-\frac{\Delta E_{ST}}{k_B T}\right)}{\frac{1}{\tau(T_1)} + \frac{1}{3\tau(S_1)}\exp\left(-\frac{\Delta E_{ST}}{k_B T}\right)} \quad (1)$$

In this equation ΔE_{ST} is the energy gap between S_1 state and T_1 state, k_B represents the Boltzmann constant, and T represents the absolute temperature. $\tau(S_1)$ and $\tau(T_1)$ are the individual decay times of the lowest singlet excited state (S_1) and the lowest triplet state (T_1). The fitting curve functionalized as eq 1 is consistent with the experimental data of decay times attained (Figure 6). The parameters are obtained by fitting with values of $\tau(S_1)$ = 562 ns, $\tau(T_1)$ = 565 μs, and ΔE_{ST} = 0.12 eV for **1** and $\tau(S_1)$ = 153 ns, $\tau(T_1)$ = 476 μs, and ΔE_{ST} = 0.12 eV for **2**. The fitted $\tau(T_1)$ values of thecomplexes **1** and **2** approximate the experimental values observed at 77 K, which are 593 and 495 μs. The calculated ΔE_{ST} values from fit curves agree quite well with the estimated values which are measured by the onsets of emission spectra at 293 and 77K. From the changes of both luminescent spectra and emission decay behaviors at different temperature we can conclude that there are two thermally equilibrated emitting states, i.e., S_1 and T_1. As shown in Figure 6, each of the fit curves shows a plateau at temperatures below 130 K. For the present cuprous complexes, the $\tau(T_1)$ lifetimes correspond to the values of the plateaus. At low enough temperatures (below 130 K, such as 77 K), the population is predominantly frozen in the T_1 state, and thus, the cuprous complexes emit almost pure phosphorescence. With temperature further increasing, gradually thermal population of the upper lying S_1 state occurs, and thus, the fit curves go downward. During this process, the emissions of these cuprous complexes stem from both S_1 and T_1 states, namely, emitting TADF and phosphorescence simultaneously. At high temperatures (>300 K), the fit curves approximate to platforms again, which implies substantial TADF emissions.

As mentioned above, both of the cuprous complexes and the pure organic ligand (PNNA) exhibit similar ILCT character (Figure 4). The large spatial overlap between the HOMO and the LUMO could lead to small ΔE_{ST}, which facilitates TADF emission.[35] In order to investigate the difference between their TADF properties, the emission properties of PNNA were measured in degassed and air-equilibrated toluene (Figure 7 and Table S3). In degassed toluene, PNNA exhibits a two-component emission decay, consisting of a nanosecond-scale prompt component (τ_p = 13 ns) and a microsecond-scale delayed component (τ_d = 58 μs). The delayed emission can be quenched by O_2 in air-equilibrated toluene. As the delayed emission has the same spectral profile as normal fluorescence from the S_1 state but with a longer decay time, the long-lived emission can be assigned to TADF. The PLQY measured in degassed toluene is 76%, which is much higher than that (29%) measured in air-equilibrated toluene. Thus, the portions of delayed fluorescence and prompt fluorescence in degassed toluene are evaluated to be 62% and 38%, respectively. Compared with pure organic compounds, prompt fluorescence of cuprous complexes can be quenched due to their faster intersystem crossing (ISC) and high spin−orbit coupling (SOC) which could result in a faster population of the triplet state.[36,37]

Electroluminescence Performance. To evaluate the electroluminescence performance of these cuprous complexes, **1** and **2** were utilized for fabricating preliminary OLEDs by solution process. The device structure is ITO (135 nm)/PEDOT:PSS (50 nm)/20 wt % cuprous complexes:80 wt % mCP (50 nm)/3TPYMB (50 nm)/LiF (0.8 nm)/Al (100 nm), for which the energy level diagrams and structure drawings of the organic materials are shown in Figure 8. mCP with good hole-transporting ability and high triplet energy level (2.93 eV) was used as host material. Moieties with excellent hole-transporting ability such as carbazole and dimethylacridine in the host and dopants should facilitate the transfer and recombination of charge carriers in the emitting layer. A thermally deposited electron-transporting/hole-blocking layer of tris[3-(3-pyridyl)mesityl]borane (3TPYMB) was employed here to confine triplet excitons and charge carriers in the emitting layer due to its high triplet energy level, excellent electron mobility, and low-lying HOMO level (−6.77 eV). HOMO/LUMO levels of the cuprous complexes were

Table 1. Photophysical Data of 1 and 2 at 293 and 77 K[a]

	1			2		
	powder[f]	in mCP film[g]	in CH_2Cl_2	powder[f]	in mCP film[g]	in CH_2Cl_2
λ_{max}[b]/nm	493 (501)	482	518	475 (516)	492	518
τ[c]/μs	145 (593)	51.7	4.6	51 (496)	48.9	7.2
Φ_{PL}[d]	60.9%	69.9%	16%	40.7%	74.6%	19%
$\Delta E(S_1-T_1)$[e]/eV	0.12			0.12		

[a] Data recorded at 77 K are given in parentheses. [b] Emission maximum. [c] Emission decay time. [d] Photoluminescence quantum yield (relative error 5%). [e] Energy gap between S_1 and T_1 states determined from temperature dependence of decay time (see Figure 6). [f] Data recorded at 77 K are given in parentheses. [g] 20 wt % in mCP thin film. Powder samples and solution samples were measured after excitation at 370 nm, and film samples were measured after excitation at 342 nm.

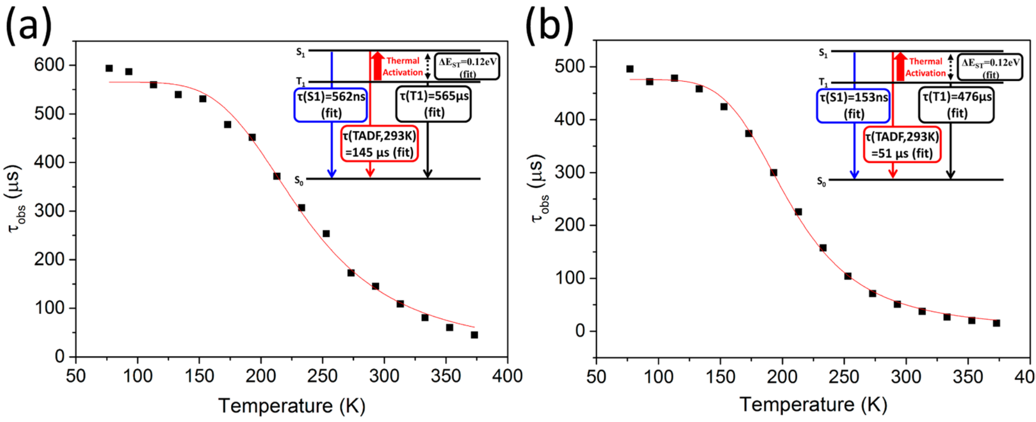

Figure 6. (a) Temperature dependence of the decay time for complex **1** powder. (b) Temperature dependence of the decay time for complex **2** powder. Solid line represents a fit curve according to eq 1. (Insets) Respective energy level diagrams for the two complexes.

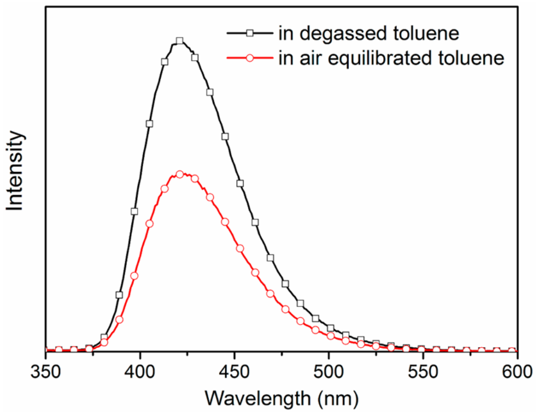

Figure 7. Emission spectra of the ligand PNNA in toluene.

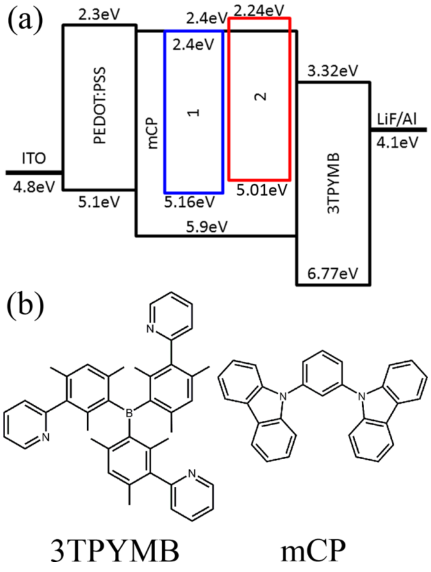

Figure 8. (a) Energy level diagrams and (b) chemical structures of the materials used in the OLED.

measured by electrochemical and optical band-gaps, which are −5.16/−2.40 eV for **1** and −5.01/−2.24 eV for **2**, respectively. The HOMO and LUMO levels of other organic materials used in the devices are obtained from the literature.[34,38,39] The device structures, including the doping concentration, the thickness of the 3TPYMB layer, and the thickness of the emitting layer, have been carefully optimized. The detailed data for device optimization are summarized in Table S4.

Figure 9 and Table 2 show the electroluminescence properties and numerical data. As shown in Figure 9a, devices of two complexes emit strong bluish-green light with peak maxima of 490 and 501 nm, respectively. No emission from the host material or other organic layers was observed, indicating efficient energy transfers between the guest and the host. Device **1** using complex **1** as dopant shows a maximum brightness of 6563 cd/m^2, peak current efficiency (CE) of 14.0 cd/A, and external quantum efficiency (EQE) of 5.83%. Device **2** based on complex **2** reaches a maximum brightness of 5579 cd/m^2, peak efficiency of 20.2 cd/A (CE), and 7.42% (EQE). The current density−voltage−brightness curves of two devices are displayed in Figure 9c. The turn-on voltages defined at a brightness of 1 cd/m^2 for devices **1** and **2** are 5.3 and 7.4 V, respectively.

The EQE of OLEDs is generally expressed by the following equation

$$\mathrm{EQE} = \gamma \times r_{\mathrm{st}} \times \Phi_{\mathrm{PL}} \times \eta_{\mathrm{coupling}} \qquad (2)$$

Herein, η_{coupling} is the light out-coupling efficiency (ca. 20−30%). The charge balance factor, γ, can be assumed to be 1 if we achieve better charge balance. r_{st} is the fraction of excitons that is allowed to decay radiatively by spin statistics. For TADF-based OLEDs, both singlet and triplet excitons can be transferred into light with a theoretical r_{st} of 100%. The two presented complexes show high PLQYs in doped host films (Φ_{PL} = 69.9% for **1** and Φ_{PL} = 74.6% for **2**). According to eq 2, much higher EQE, i.e., EQE = 14−21% for **1**-based OLED and EQE = 14.9−22.4% for **2**-based OLED, could be expected for OLEDs based on these complexes. From this perspective, the device structure and functional layer materials should be further optimized to achieve better device performance. In order to effectively evaluate the current device performance, two representative analogous complexes and corresponding OLEDs have been chosen from refs 34 and 40 for comparison. The PLQYs and device performance of these complexes are listed in Table S4. Among these analogous cuprous complexes, complex **2** in this work shows the highest PLQY in host film, which may be due to its rigid and bulky ligands. Besides, the bluest electroluminescence and highest brightness have been realized in the device containing complex **2**. Although complex

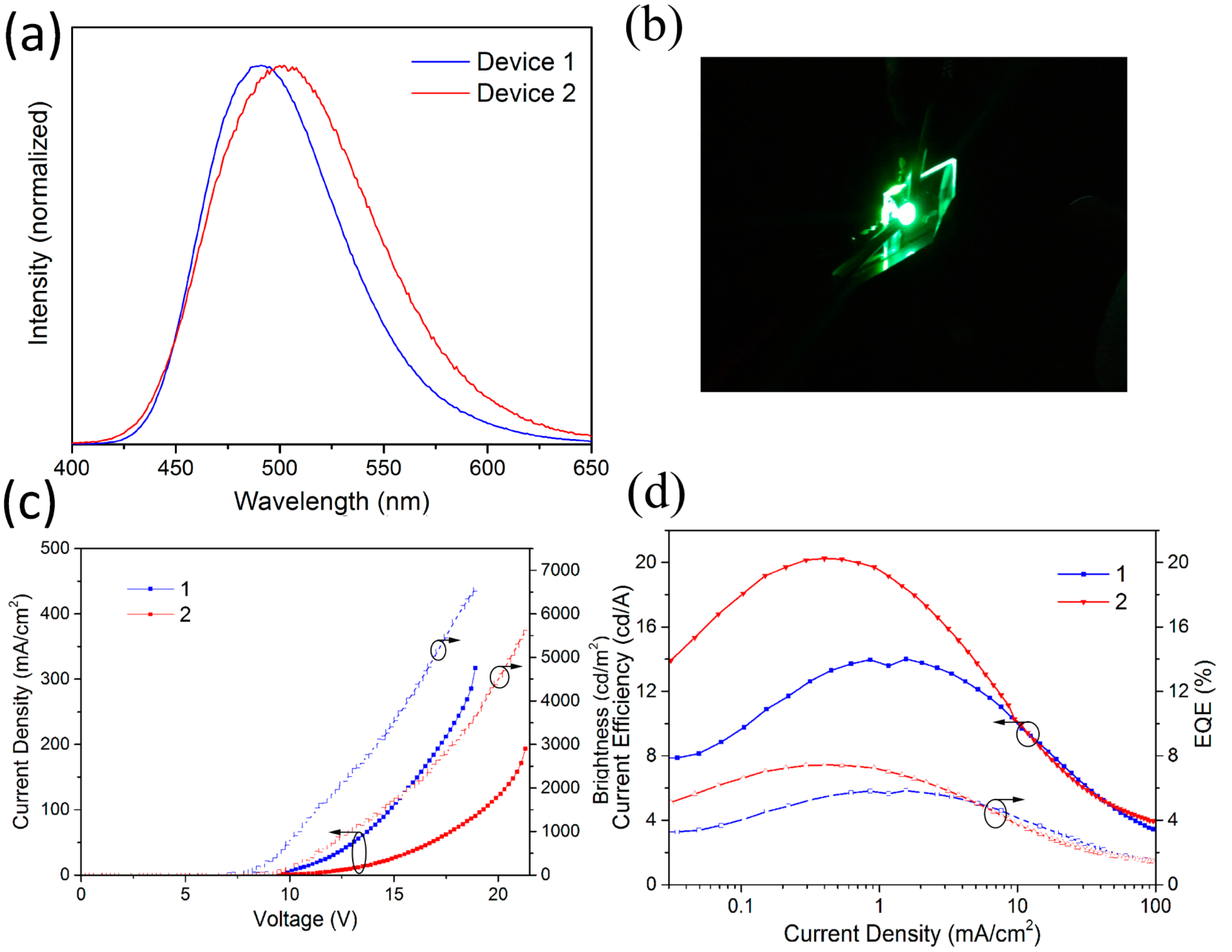

Figure 9. (a) EL spectra; (b) image of device 2; (c) current density−voltage−brightness (*I*−*V*−*B*) curves; (d) plots of external quantum efficiency and current efficiency vs brightness.

Table 2. EL Characteristics of the OLEDs

	EQE (%)		CE (cd/A)		V_{on} (V)			
	max	@100 cd/m^2	max	@100 cd/m^2	@1 cd/m^2	B_{max} (cd/m^2)	λ (nm)	CIE1931 (*x*, *y*)
device 1	5.83	5.70	14.01	13.71	5.3	6563	490	(0.166, 0.370)
device 2	7.42	7.41	20.24	20.20	7.4	5579	501	(0.206, 0.426)

2 exhibits the highest PLQY, the efficiencies of complex **2**-based device are moderate and still need to be improved.

■ CONCLUSIONS

In conclusion, two highly efficient cuprous complexes with bluish-green luminescence have been designed and synthesized by using a functional diimine ligand. These complexes emit efficient TADF at room temperature. High efficiencies up to 20.24 cd/A (CE), 7.42% (EQE), and a peak brightness of 5579 cd/cm^2 were realized in the solution-processed OLED based on complex **2** thanks to the confinement of triplet excitons and charge carriers. Nonetheless, the devices should be further optimized to realize better performance, especially higher efficiencies and lower turn-on voltage. This work is currently in progress in our lab. The functional dimethylacridine moiety on the diimine ligand not only could lead to the uncommon ILCT transition for the cuprous complexes but also facilitates the transfer and recombination of charge carriers in the emitting layer. Improved photoluminescence and electroluminescence performance together with special photophysical properties could be expected for cuprous complexes by introducing some functional moieties in the ligands. The encouraging results combined with rational design strategies in this study may provide a guide for developing highly efficient cuprous complexes and OLEDs.

■ EXPERIMENTAL SECTION

General Procedures. All reactions were performed under N_2 atmosphere using standard Schlenk techniques unless specified. Chemicals were purchased from commercial sources and without further purification. Solvents were freshly distilled over appropriate drying reagents. The complex $[Cu(CH_3CN)_4]BF_4$ was prepared by the literature procedure.[41] PEDOT:PSS was purchased from Heraeus. ^1H NMR and ^{31}P NMR spectra were recorded on a Bruker Avance III 400 MHz NMR spectrometer. Elemental analyses (C, H, N) were carried out with an Elementar Vario EL III elemental analyzer.

Synthesis and Characterization. *Synthesis of 3-Phenyl-1H-pyrazole.* To a Schlenk tube with a magnetic bar was added cinnamaldehyde (50 mmol), *p*-toluenesulfonyl hydrazide (60 mmol, 1.2 equiv), NaOH (1.5 equiv), (n-Bu)$_4$NBr (1.5 equiv), and distilled water (200 mL). The reaction mixture was refluxed for 10 h in an oil bath. After cooling to room temperature, the reaction mixture was extracted and washed with CH_2Cl_2 and brine and then dried over sodium sulfate. The crude product was purified by column chromatography on silica gel to afford a white solid (6.4 g, 89%).

Synthesis of 5-Bromo-2-(3-phenyl-1H-pyrazol-1-yl)pyridine. 3-Phenyl-1*H*-pyrazole (5 mmol) was added to a Schlenk tube filled with distilled DMAC (20 mL), followed by addition of anhydrous K_2CO_3 (10 mmol). Then 5-bromo-2-fluoropyridine (5 mmol) was added to the mixture after the solution was stirred at room temperature for 30 min. The mixture was reflux for 8 h in a 180 °C oil bath. After cooling the mixture was extracted and washed with CH_2Cl_2/brine. After being dried over sodium sulfate, the crude product was purified by column chromatography on silica gel to afford a white solid (1.44g, 96%). ^{1}H NMR (400 MHz, $CDCl_3$): δ 8.54 (d, J = 2.6 Hz, 1H), 8.45 (d, J = 1.9 Hz, 1H), 8.02 (d, J = 8.7 Hz, 1H), 7.92 (d, J = 8.5 Hz, 3H), 7.45 (t, J = 7.5 Hz, 2H), 7.37 (t, J = 7.3 Hz, 1H), 6.80 (s, 1H).

Synthesis of 9,9-Dimethyl-10-(6-(3-phenyl-1H-pyrazol-1-yl)-pyridin-3-yl)-9,10-dihydroacridine (PNNA). To a solution of 5-bromo-2-(3-phenyl-1*H*-pyrazol-1-yl)pyridine (2 mmol) in distilled toluene (8 mL) was added NaO^{t}Bu (2 mmol) and Pd(OAc)$_2$ (0.05 mmol, 11 mg), followed by the addition of P(t-Bu)$_3$BF$_4$ (0.2 mmol, 0.058g). The mixture was stirred for 30 min. Then 9,9-dimethylacridan (2 mmol) was added to the reaction tube. The reaction mixture was refluxed for 6 h at 120 °C in an oil bath. When the reaction was carried out for 6 h, 1,1′-bis(diphenylphosphino)ferrocene (DPPF, 0.1 mmol 0.055g) was added to that hot mixture under N_2 atmosphere. Then the reaction continued to reflux for 12 h. After cooling to room temperature, the solvent was removed by vacuum−rotary evaporation. The mixture was extracted and washed with CH_2Cl_2 and brine. After being dried over sodium sulfate, the crude product was purified by column chromatography on silica gel to afford a light yellow solid (0.72g, 84%). ^{1}H NMR (400 MHz, $CDCl_3$): δ 8.68 (d, J = 2.6 Hz, 1H), 8.40 (dd, J = 7.2, 5.9 Hz, 2H), 7.98 (dd, J = 8.3, 1.1 Hz, 2H), 7.86 (dd, J = 8.6, 2.5 Hz, 1H), 7.49 (ddd, J = 12.4, 6.3, 4.6 Hz, 4H), 7.39 (ddd, J = 8.4, 2.4, 1.2 Hz, 1H), 7.00 (m, 4H), 6.86 (d, J = 2.7 Hz, 1H), 6.32 (dd, J = 7.9, 1.4 Hz, 2H), 1.72 (s, 6H).

Synthesis of Cuprous Complexes. The two cuprous complexes **1** and **2** were prepared according to the following general procedure: a mixture of $[Cu(CH_3CN)_4]BF_4$ and the corresponding phosphine ligand (1 mmol POP or 1 mmol Xantphos) in CH_2Cl_2 (5 mL) was stirred for 30 min at room temperature, and then PNNA (1 mmol) was added. After the mixture was stirred for another hour, the solvent was removed by evaporation. Single crystals of these two complexes suitable for X-ray diffraction measurements were obtained by diffusion of ether into CH_2Cl_2 solution of the cuprous complexes.

*[Cu(czpzpy)(POP)]BF$_4$ (**1**).* ^{1}H NMR (400 MHz, $CDCl_3$): δ 9.04 (s, 1H), 8.57 (d, J = 8.7 Hz, 1H), 8.10 (d, J = 8.5 Hz, 1H), 7.66−7.57 (m, 3H), 7.41 (d, J = 7.0 Hz, 3H), 7.07 (dd, J = 15.9, 8.2 Hz, 8H), 7.02−6.88 (m, 7H), 6.88−6.70 (m, 10H), 6.61 (d, J = 7.8 Hz, 2H), 5.81 (d, J = 8.1 Hz, 2H), 5.30 (s, 1H), 3.72 (q, J = 7.0 Hz, 4H), 3.48 (q, J = 7.0 Hz, 1H), 1.23 (m, 8H). ^{31}P NMR (162 MHz, $CDCl_3$): δ −12.10 (s). Anal. Calcd for $C_{65}H_{52}BCuF_4N_4OP_2\cdot 0.5(H_2O)\cdot 0.5(CH_2Cl_2)$: C, 67.30; H,4.66; N, 4.79. Found: C, 66.98; H, 4.71; N, 4.68.

*[Cu(czpzpy)(Xantphos)]BF$_4$ (**2**).* ^{1}H NMR (400 MHz, $CDCl_3$): δ 7.63 (d, J = 7.4 Hz, 1H), 7.42 (d, J = 7.6 Hz, 1H), 7.37−7.28 (m, 2H), 7.22 (t, J = 7.2 Hz, 2H), 7.08 (m, 5H), 6.97−6.56 (m, 9H), 6.39 (s, 1H), 5.49 (d, J = 8.1 Hz, 1H), 3.72 (q, J = 7.0 Hz, 8H), 1.63 (s, 3H), 1.48 (s, 9H), 1.24 (t, J = 7.0 Hz, 13H). ^{31}P NMR (162 MHz, $CDCl_3$): δ −11.86 (s). Anal. Calcd for $C_{68}H_{56}BCuF_4N_4OP_2$: C, 70.56; H, 4.88; N, 4.84. Found: C, 69.87; H, 4.78; N, 4.79.

Electrochemical Measurements. Cyclic voltammetry measurements were performed in a gastight single-compartment three-electrode cell with a BAS Epsilon Electrochemical Analyzer at room temperature. A glassy carbon disk and a platinum wire were selected as the working and auxiliary electrodes, respectively. The reference electrode was Ag/Ag$^+$ (0.1 M of $AgNO_3$ in CH_2Cl_2). The CV measurements were carried out in anhydrous and nitrogen-saturated CH_2Cl_2 solutions with 0.1 M n-tetrabutylammonium perchlorate (TBAP) and 1.0 mM cuprous complex. The ferrocenium/ferrocene couple was used as an internal standard.

Photophysical Measurements. UV−vis absorption spectra were recorded with a PerkinElmer Lambda 45 UV−vis spectrophotometer. Photoluminescence spectra at each temperature were recorded on a HORIBA Jobin-Yvon FluoroMax-4 instrument. The lifetimes at different temperatures were acquired on a HORIBA Jobin-Yvon FluoroMax-4 instrument with a multichannel scaling (MCS) peripheral equipment and a spectraLED (373 nm). The PL quantum yields were defined as the number of photons emitted per photon absorbed by the system and measured using a HORIBA Jobin-Yvon FluoroMax-4 instrument equipped with an integrating sphere.

X-ray Crystallographic Analysis. Diffraction data for two complexes were collected on a SuperNova, Dual, Cu at zero, Atlas diffractometer equipped with graphite-monochromated Cu Kα radiation (λ = 1.54184 Å). Structures were solved by direct methods and refined by full-matrix least-squares methods using the SHELXL-97 program package. Hydrogen atoms were added in idealized positions. All nonhydrogen atoms were refined anisotropically. Details of the crystal and structure refinements are listed in Table S1. Selected bond lengths and bond angles are listed in Table S2 in the Supporting Information for complexes **1** and **2**. CCDC 1454914 and 1454915 contain the supplementary crystallographic data for complexes**1** and **2**, respectively.

Computational Methodology. Calculations on the electronic structures of **1** and **2** were carried out using density functional theory (DFT) with the B3LYP hybrid functional.[42,43] A "double-ζ" quality basis set consisting of Hay and Wadt's effective core potentials (LANL2DZ)[44−46] was employed for the C, N, O, and H atoms, and a LANL08 basis set[47] was employed for the Cu and P atoms. Time-dependent DFT (TDDFT) calculations using the B3LYP functional were then performed on the optimized structures at ground states.[48−52] All calculations were carried out using Gaussian 03.[53]

Device Fabrication and Characterization. The hole-blocking material tris[3-(3-pyridyl)mesityl]borane (3TPYMB) was prepared by a literature procedure, and PNNA was synthesized as above mentioned. All compounds were purified by sublimation after recrystallization. Poly(3,4-ethylene dioxythiophene):poly(styrene sulfonic acid) (PEDOT:PSS) was purchased from Heraeus and filtered through a 0.22 μm filter before use. Other materials used in the device fabrication were purchased from commercial sources and used without further purification. A 40 nm thick PEDOT:PSS film was first spin coated (at 4800 rpm) on a precleaned ITO-glass substrate and then dried at 125 °C for 25 min. The emitting layer was then overlaid by spin coating (at 2100 rpm) a filtered 5.5 mg mL^{-1} CH_2Cl_2 solution of a mixture of host and dopant (for device **1**, 2 mg of complex **1** and 8 mg of mCP dissolved in 1.8 mL of CH_2Cl_2; for device **2**: 2 mg of complex **2** and 8 mg of mCP dissolved in 1.8 mL of CH_2Cl_2). The film was then dried under a vacuum for 1 h at room temperature. Successively, 10 nm of 3TPYMB, 50 nm TPBI, 0.8 nm of LiF, and 100 nm of Al were deposited in an inert chamber at a base pressure of less than 4×10^{-4} Pa. The electroluminescence (EL) spectra were recorded on a HORIBA Jobin-Yvon FluoroMax-4 spectrometer. The current density−voltage−brightness (I−V−B) curves of the devices were recorded on a Keithley 2400/2000 source meter and a calibrated silicon photodiode. All measurements on the devices were carried out at room temperature.

■ ASSOCIATED CONTENT

Supporting Information

The Supporting Information is available free of charge on the ACS Publications website at DOI: 10.1021/acs.inorgchem.6b00763.

(CIF)

(CIF)

Necessary experimental data (PDF)

AUTHOR INFORMATION

Corresponding Author

*E-mail: czlu@fjirm.ac.cn.

Present Address

Fujian Institute of Research on the Structure of Matter, Chinese Academy of Sciences, Fuzhou, Fujian, 350002, P. R. China.

Author Contributions

All authors have given approval to the final version of the manuscript.

Notes

The authors declare no competing financial interest.

ACKNOWLEDGMENTS

This work was supported by the 973 key program of the Chinese Ministry of Science and Technology (MOST) (2012CB821705), the Chinese Academy of Sciences (KJCX2-YW-319, KJCX2-EW-H01), the National Natural Science Foundation of China (21373221, 21521061, 91122027, 51172232, 21403236), and the Natural Science Foundation of Fujian Province (2012J06006, 2014J05026, 2006L2005).

REFERENCES

(1) Lee, J.; Chen, H. F.; Batagoda, T.; Coburn, C.; Djurovich, P. I.; Thompson, M. E.; Forrest, S. R. *Nat. Mater.* **2015**, *15*, 92−98.

(2) Ma, Y.; Zhang, H.; Shen, J.; Che, C. *Synth. Met.* **1998**, *94*, 245−248.

(3) Yersin, H.; Rausch, A. F.; Czerwieniec, R. *Physics of Organic Semiconductors*; Wiley-VCH Verlag: New York, 2012; pp 371−424.

(4) Leitl, M. J.; Krylova, V. A.; Djurovich, P. I.; Thompson, M. E.; Yersin, H. *J. Am. Chem. Soc.* **2014**, *136*, 16032−16038.

(5) Volz, D.; Chen, Y.; Wallesch, M.; Liu, R.; Flechon, C.; Zink, D. M.; Friedrichs, J.; Flugge, H.; Steininger, R.; Gottlicher, J.; Heske, C.; Weinhardt, L.; Brase, S.; So, F.; Baumann, T. *Adv. Mater.* **2015**, *27*, 2538−2543.

(6) Chen, X. L.; Yu, R.; Zhang, Q. K.; Zhou, L. J.; Wu, X. Y.; Zhang, Q.; Lu, C. Z. *Chem. Mater.* **2013**, *25*, 3910−3920.

(7) Zink, D. M.; Volz, D.; Baumann, T.; Mydlak, M.; Flügge, H.; Friedrichs, J.; Nieger, M.; Bräse, S. *Chem. Mater.* **2013**, *25*, 4471−4486.

(8) Zink, D. M.; Bachle, M.; Baumann, T.; Nieger, M.; Kuhn, M.; Wang, C.; Klopper, W.; Monkowius, U.; Hofbeck, T.; Yersin, H.; Brase, S. *Inorg. Chem.* **2013**, *52*, 2292−2305.

(9) Liu, Z. W.; Qayyum, M. F.; Wu, C.; Whited, M. T.; Djurovich, P. I.; Hodgson, K. O.; Hedman, B.; Solomon, E. I.; Thompson, M. E. *J. Am. Chem. Soc.* **2011**, *133*, 3700−3703.

(10) Hashimoto, M.; Igawa, S.; Yashima, M.; Kawata, I.; Hoshino, M.; Osawa, M. *J. Am. Chem. Soc.* **2011**, *133*, 10348−10351.

(11) Leitl, M. J.; Küchle, F.-R.; Mayer, H. A.; Wesemann, L.; Yersin, H. *J. Phys. Chem. A* **2013**, *117*, 11823−11836.

(12) Osawa, M. *Chem. Commun.* **2014**, *50*, 1801−1803.

(13) Liu, Z.; Qiu, J.; Wei, F.; Wang, J.; Liu, X.; Helander, M. G.; Rodney, S.; Wang, Z.; Bian, Z.; Lu, Z.; Thompson, M. E.; Huang, C. *Chem. Mater.* **2014**, *26*, 2368−2373.

(14) Hofbeck, T.; Monkowius, U.; Yersin, H. *J. Am. Chem. Soc.* **2015**, *137*, 399−404.

(15) Deaton, J. C.; Switalski, S. C.; Kondakov, D. Y.; Young, R. H.; Pawlik, T. D.; Giesen, D. J.; Harkins, S. B.; Miller, A. J.; Mickenberg, S. F.; Peters, J. C. *J. Am. Chem. Soc.* **2010**, *132*, 9499−9508.

(16) Osawa, M.; Kawata, I.; Ishii, R.; Igawa, S.; Hashimoto, M.; Hoshino, M. *J. Mater. Chem. C* **2013**, *1*, 4375−4383.

(17) Bizzarri, C.; Strabler, C.; Prock, J.; Trettenbrein, B.; Ruggenthaler, M.; Yang, C. H.; Polo, F.; Iordache, A.; Bruggeller, P.; De Cola, L. *Inorg. Chem.* **2014**, *53*, 10944−10951.

(18) Czerwieniec, R.; Yu, J.; Yersin, H. *Inorg. Chem.* **2011**, *50*, 8293−8301.

(19) Yersin, H.; Rausch, A. F.; Czerwieniec, R.; Hofbeck, T.; Fischer, T. *Coord. Chem. Rev.* **2011**, *255*, 2622−2652.

(20) Chen, X. L.; Lin, C.-S.; Wu, X. Y.; Yu, R.; Teng, T.; Zhang, Q. K.; Zhang, Q.; Yang, W. B.; Lu, C. Z. *J. Mater. Chem. C* **2015**, *3*, 1187−1195.

(21) Zhang, Q.; Chen, X. L.; Chen, J.; Wu, X. Y.; Yu, R.; Lu, C. Z. *RSC Adv.* **2015**, *5*, 34424−34431.

(22) Zhang, Q.; Chen, X. L.; Chen, J.; Wu, X. Y.; Yu, R.; Lu, C. Z. *Dalton Trans.* **2015**, *44*, 10022−10029.

(23) Zhang, Q.; Chen, J.; Wu, X. Y.; Chen, X. L.; Yu, R.; Lu, C. Z. *Dalton Trans.* **2015**, *44*, 6706−6710.

(24) Chiba, T.; Pu, Y. J.; Kido, J. *Adv. Mater.* **2015**, *27*, 4681−4687.

(25) Xu, L. J.; Wang, J.-Y.; Zhu, X. F.; Zeng, X. C.; Chen, Z. N. *Adv. Funct. Mater.* **2015**, *25*, 3033−3042.

(26) Yook, K. S.; Lee, J. Y. *Adv. Mater.* **2014**, *26*, 4218−4233.

(27) Yook, K. S.; Lee, J. Y. *Adv. Mater.* **2012**, *24*, 3169−3190.

(28) Cho, Y. J.; Yook, K. S.; Lee, J. Y. *Adv. Mater.* **2014**, *26*, 6642−6646.

(29) Yook, K. S.; Lee, J. Y. *Adv. Mater.* **2014**, *26*, 4218−4233.

(30) Wong, W. Y.; Ho, C. L. *Coord. Chem. Rev.* **2009**, *253*, 1709−1758.

(31) Wang, X.; Wang, S.; Ma, Z.; Ding, J.; Wang, L.; Jing, X.; Wang, F. *Adv. Funct. Mater.* **2014**, *24*, 3413−3421.

(32) Xia, D.; Wang, B.; Chen, B.; Wang, S.; Zhang, B.; Ding, J.; Wang, L.; Jing, X.; Wang, F. *Angew. Chem., Int. Ed.* **2014**, *53*, 1048−1052.

(33) Wang, Y.; Wang, S.; Zhao, N.; Gao, B.; Shao, S.; Ding, J.; Wang, L.; Jing, X.; Wang, F. *Polym. Chem.* **2015**, *6*, 1180−1191.

(34) Hsu, C. W.; Lin, C. C.; Chung, M. W.; Chi, Y.; Lee, G. H.; Chou, P. T.; Chang, C. H.; Chen, P. Y. *J. Am. Chem. Soc.* **2011**, *133*, 12085−12099.

(35) Endo, A.; Sato, K.; Yoshimura, K.; Kai, T.; Kawada, A.; Miyazaki, H.; Adachi, C. *Appl. Phys. Lett.* **2011**, *98*, 083302.

(36) Bergmann, L.; Hedley, G. J.; Baumann, T.; Brase, S.; Samuel, I. D. *Sci. Adv.* **2016**, *2*, e1500889.

(37) Chen, X. L.; Yu, R.; Wu, X. Y.; Liang, D.; Jia, J. H.; Lu, C. Z. *Chem. Commun.* **2016**, *52*, 6288−6291.

(38) Zhang, Q.; Ding, J.; Cheng, Y.; Wang, L.; Xie, Z.; Jing, X.; Wang, F. *Adv. Funct. Mater.* **2007**, *17*, 2983−2990.

(39) Lee, S. Y.; Yasuda, T.; Nomura, H.; Adachi, C. *Appl. Phys. Lett.* **2012**, *101*, 093306.

(40) Zhang, Q.; Komino, T.; Huang, S.; Matsunami, S.; Goushi, K.; Adachi, C. *Adv. Funct. Mater.* **2012**, *22*, 2327−2336.

(41) Kubas, G. J. *Inorg. Synth.* **1990**, *28*, 68−70.

(42) Lee, C.; Yang, W.; Parr, R. G. *Phys. Rev. B: Condens. Matter Mater. Phys.* **1988**, *37*, 785−789.

(43) Becke, A. D. *J. Chem. Phys.* **1993**, *98*, 5648−5652.

(44) Hay, P. J.; Wadt, W. R. *J. Chem. Phys.* **1985**, *82*, 270−283.

(45) Wadt, W. R.; Hay, P. J. *J. Chem. Phys.* **1985**, *82*, 284−298.

(46) Hay, P. J.; Wadt, W. R. *J. Chem. Phys.* **1985**, *82*, 299−310.

(47) Roy, L. E.; Hay, P. J.; Martin, R. L. *J. Chem. Theory Comput.* **2008**, *4*, 1029−1031.

(48) Petersilka, M.; Gossmann, U. J.; Gross, E. K. U. *Phys. Rev. Lett.* **1996**, *76*, 1212−1215.

(49) Bauernschmitt, R.; Ahlrichs, R.; Hennrich, F. H.; Kappes, M. M. *J. Am. Chem. Soc.* **1998**, *120*, 5052−5059.

(50) Stratmann, R. E.; Scuseria, G. E.; Frisch, M. J. *J. Chem. Phys.* **1998**, *109*, 8218−8224.

(51) Jamorski, C.; Casida, M. E.; Salahub, D. R. *J. Chem. Phys.* **1996**, *104*, 5134−5147.

(52) Casida, M. E.; Jamorski, C.; Casida, K. C.; Salahub, D. R. *J. Chem. Phys.* **1998**, *108*, 4439−4449.

(53) Frisch, M. J.; Trucks, G. W.; Schlegel, H. B.; Scuseria, G. E.; Robb, M. A.; Cheeseman, J. R.; Montgomery, J. A. J.; Vreven, T.; Kudin, K. N.; Burant, J. C.; Millam, J. M.; Iyengar, S. S.; Tomasi, J.; Barone, V.; Mennucci, B.; Cossi, M.; Scalmani, G.; Rega, N.; Petersson, G. A.; Nakatsuji, H.; Hada, M.; Ehara, M.; Toyota, K.; Fukuda, R.; Hasegawa, J.; Ishida, M.; Nakajima, T.; Honda, Y.; Kitao, O.; Nakai, H.; Klene, M.; Li, X.; Knox, J. E.; Hratchian, H. P.; Cross, J. B.; Adamo, C.; Jaramillo, J.; Gomperts, R.; Stratmann, R. E.; Yazyev, O.; Austin, A. J.; Cammi, R.; Pomelli, C.; Ochterski, J. W.; Ayala, P. Y.;

DOI: 10.1021/acs.inorgchem.6b00763

Morokuma, K.; Voth, G. A.; Salvador, P.; Dannenberg, J. J.; Zakrzewski, V. G.; Dapprich, S.; Daniels, A. D.; Strain, C.; Farkas, M. O.; Malick, D. K.; Rabuck, A. D.; Raghavachari, K.; Foresman, J. B.; Ortiz, J. V.; Cui, Q.; Baboul, A. G.; Clifford, S., Cioslowski, J.; Stefanov, B. B.; Liu, G.; Liashenko, A.; Piskorz, P.; Komaromi, I.; Martin, R. L.; Fox, D. J.; Keith, T.; Al-Laham, M. A., Peng, C. Y.; Nanayakkara, A.; Challacombe, M.; Gill, P. M. W.; Johnson, B.; Chen, W.; Wong, M. W.; Gonzalez, C.; Pople, J. A. *Gaussian 03*; Gaussian Inc.: Willingford, CT, 2003.

DOI: 10.1021/acs.inorgchem.6b00763
Inorg. Chem. XXXX, XXX, XXX−XXX